

## Angle-resolved soft-x-ray fluorescence and absorption study of graphite

P. Skytt, P. Glans, D. C. Mancini, J.-H. Guo, N. Wassdahl, and J. Nordgren  
*Department of Physics, Uppsala University, Box 530, S-751 21 Uppsala, Sweden*

Y. Ma

*Physics Department, University of Washington, Seattle, Washington 98195  
 and Molecular Science Research Centre, Pacific Northwest Laboratories, Richland, Washington 99352*  
 (Received 29 April 1994)

The x-ray fluorescence and absorption of highly oriented pyrolytic graphite have been measured using monochromatic synchrotron radiation. The spectra can be separated into contributions from  $\pi$ - and  $\sigma$ -band components by measuring at different angles of incidence and at different emission angles. The shape of the x-ray fluorescence spectra varies dramatically with excitation energy near the C *K* edge. This dependence on excitation energy can be interpreted within a resonant-inelastic-scattering formalism. The results are compared with previously published band-structure calculations and photoemission results, and demonstrate the potential for using x-ray fluorescence to obtain symmetry-resolved band information.

### I. INTRODUCTION

X-ray emission spectroscopy (XES) and x-ray absorption spectroscopy (XAS) are traditionally used for studying the occupied and unoccupied density of states (DOS), respectively. The development of new photon excitation sources using synchrotron radiation (SR), yielding high flux of high-resolution monochromatic soft x rays, makes new types of experiments possible today. For example, it has recently been demonstrated for diamond that band-structure information, previously obtained by various photoemission techniques<sup>1</sup> as well as x-ray scattering,<sup>2</sup> can be obtained with a combination of XAS and XES measurements<sup>3,4</sup> using a resonant inelastic x-ray scattering (RIXS) interpretation.<sup>5</sup>

The valence electronic structure of graphite has been investigated extensively because of its interesting two-dimensional character. The occupied DOS has been examined experimentally using x-ray photoemission spectroscopy (XPS),<sup>6</sup> ultraviolet photoemission spectroscopy,<sup>7</sup> and XES.<sup>8,9</sup> The unoccupied DOS has been examined by inverse photoemission spectroscopy<sup>10,11</sup> and XAS.<sup>12-15</sup> Momentum information has been obtained experimentally using angle-resolved photoemission spectroscopy (ARPES),<sup>16</sup> angle-resolved inverse photoemission spectroscopy,<sup>10,11</sup> and inelastic x-ray scattering.<sup>2</sup> Using polarization-dependent XAS for the unoccupied DOS,<sup>13</sup> it has been possible to obtain a separation of  $\sigma$  and  $\pi$  states. This separation for the occupied DOS can be obtained using angle-resolved XES.<sup>9</sup>

The valence states in graphite have predominantly  $2s$  and  $2p$  symmetry and can be divided into states with one of the two different molecular orbital characteristics. The  $2s$  and  $2p$  distributions in the valence band are well known. The  $2s$  electrons contribute to the lower-energy part and the  $2p$  electrons are at the higher energies with a substantial hybridization in the middle region.<sup>17</sup> Due to the layering of the crystal structure, the bands can be di-

vided into two different symmetries: the  $\sigma$  states, contributed to by the  $2s$ ,  $2p_x$ , and  $2p_y$  atomic orbitals, lying in the planes, and the  $\pi$  states, consisting of the  $2p_z$  orbitals, oriented perpendicular to the planes. Band-structure calculations<sup>18,19</sup> and results from XES (Ref. 9) have shown that the low-energy region of the valence band is of  $\sigma$  character, while the high-energy region has mainly  $\pi$  character.

### II. EXPERIMENTAL

The experiments were carried out at the X1B beamline of the National Synchrotron Light Source at Brookhaven National Laboratory. A spherical-grating monochromator with the X1 undulator as its source provided intense, linearly polarized, high-resolution monochromatic soft x-ray radiation.<sup>20</sup> The C *K* emission spectra were recorded with a grazing-incidence, spherical-grating spectrometer<sup>21</sup> mounted with its optical axis perpendicular to the incident x-ray beam and in the direction of the polarization vector. For fluorescence measurements, the bandpass of the excitation source was set to about 0.3 eV, full width at half maximum (FWHM), near the C *K* edge and the resolution of the spectrometer was set to about 0.5 eV FWHM. The latter value was determined by measuring the specular reflection from the sample with a bandpass set to less than 0.1 eV FWHM for the monochromator. Measuring the energy of the reflected beam established a consistent energy scale for the absorption and fluorescence spectra. The spectrometer was calibrated for energy using electron-excited *L* emission for Zn and Cr recorded in higher order of diffraction. The highly oriented pyrolytic graphite (HOPG) sample, cut with the surface in the basal plane, was cleaved using adhesive tape to obtain a fresh surface immediately before mounting it in the vacuum chamber. Fluorescence and absorption spectra were recorded with the sample at three different angles, 12°, 32°, and 72°, measured between the

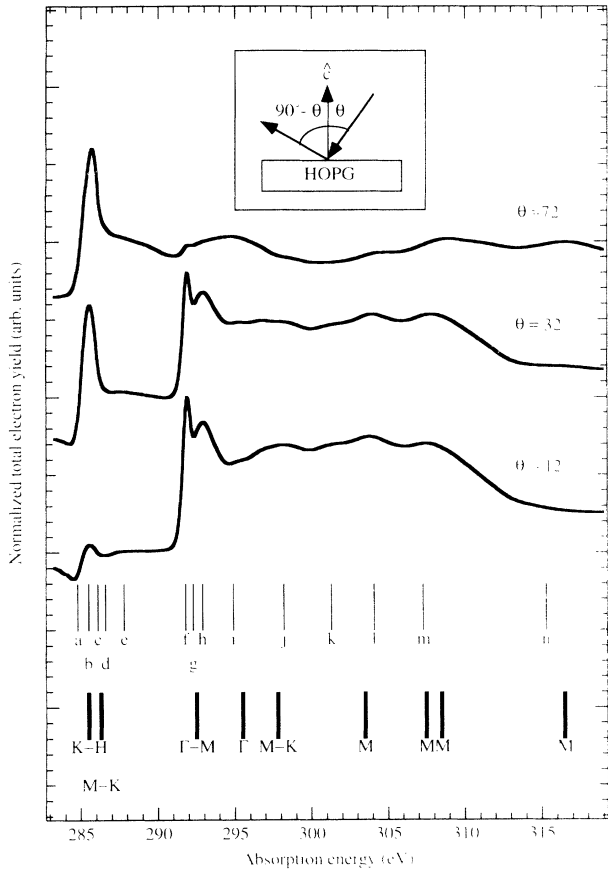


FIG. 1. X-ray absorption data recorded measuring the total electron yield from the sample. The incidence angles ( $\theta$ ) of the three spectra are indicated in the figure. The bars labeled with lower-case letters indicate where x-ray emission spectra have been recorded and the bars labeled with upper-case letters indicate critical points in the absorption final state according to identifications by Rosenberg, Love, and Rehn (Ref. 13).

Poynting vector of the incident x-ray beam and the sample's surface normal (the  $c$  axis). The corresponding angles between the  $c$  axis and the detected emission were  $78^\circ$ ,  $58^\circ$ , and  $18^\circ$ , respectively (Fig. 1, inset). The C  $K$  absorption spectra were measured by scanning the monochromator while monitoring the total photocurrent from the sample and normalizing this signal to the incoming flux, as measured by the total photocurrent from a clean gold mesh.

### III. RESULTS AND DISCUSSION

The angular dependence for x-ray absorption and emission from graphite and other anisotropic materials is fairly well understood. Both x-ray emission and absorption in the case of graphite probe only electrons with  $p$  symmetry, which makes XES and XAS useful for determination of  $p$ -type partial DOS's. When  $\pi$  electrons fill the core vacancy, the x rays are emitted in a dipole pattern such that no  $\pi$  emission is emitted along the  $c$  axis. The photons emitted by electrons filling the core hole from  $\sigma$  states, on the other hand, are emitted in all directions, but strongest in the direction of the  $c$  axis. It is possible,

using angle-resolved XES, to separate the emission from the  $\sigma$  and  $\pi$  states.<sup>8</sup> Specifically, in the dipole approximation, the intensity of the  $\sigma$  and  $\pi$  contributions can be separated from spectra recorded at different angles with respect to the  $c$  axis. Extraction of  $\sigma$  and  $\pi$  contributions to the graphite spectrum has been done previously,<sup>8</sup> and the emission from the  $\sigma$  states contributes to the low-energy part of the spectrum with a maximum at  $\sim 275$  eV and intensity up to  $\sim 280$  eV, while the  $\pi$  states contribute to the high-energy part from the Fermi level down to  $\sim 275$  eV with a maximum at  $\sim 282$  eV.

Figure 1 displays the absorption spectra obtained at three different incidence angles. The vertical bars in the figure which are labeled with lower-case letters indicate the energies at which XES spectra were recorded. The critical points of the absorption final states are indicated using Refs. 13 and 22. The absorption spectra agree well with previously published results,<sup>12–15</sup> especially with the spectra recorded by Terminello *et al.*<sup>14</sup> and Batson,<sup>15</sup> which are recorded at about the same instrumental resolution. It should be noted that the sharp feature appearing at excitation energy 292 eV, labeled  $f$ , is not due to the band structure but to an excitonic state.<sup>23</sup> When the polarization vector of the incident beam is parallel to the basal plane only excitations to  $\sigma$  states are possible. Excitations to  $\pi$  states becomes more likely the more perpendicular to the basal plane the polarization vector is. Thus, comparing the spectra in Fig. 1, one can see that the main feature below 290 eV has mainly  $\pi$  character since it is quenched at near-normal incidence, while the  $\sigma$  states are observed at energies above 292 eV.

Figure 2 displays fluorescence spectra recorded at various excitation energies and at three different angles. Different angles are obtained by rotation of the sample around an axis perpendicular to the  $c$  axis and to the direction of the incoming beam. The incidence angles were  $12^\circ$ ,  $32^\circ$ , and  $72^\circ$ , according to the definition shown in the inset in Fig. 1. The spectra have been normalized to have the same intensity at the low-energy flank. The shapes of the spectra indicate a strong dependence on both angle and excitation energy. The variation with emission angle is similar to what is seen in emission spectra with excitation by electrons or high-energy photons,<sup>9</sup> and it is due to the difference in intensity distribution between  $\sigma$  and  $\pi$  components of the emission. The variation with excitation energy is more complicated. While there are only minor changes in the energy of the features appearing in the fluorescence spectra, there are large variations in their relative intensities. There are strong changes in the fluorescence spectra for excitation energies near the absorption threshold, and lesser but still apparent variations as much as 20 eV above the threshold. In Fig. 2, with the excitation energy equal to the lowest-energy  $\pi$  absorption peak at 285.5 eV (curve b), the  $\sigma$  component of the emission has a pronounced peak at 272.5 eV, while the  $\pi$  component has one at 283 eV. When the excitation energy is increased by 1.1 eV to 286.1 eV (curve d), the emission profile changes significantly. For the  $\sigma$  component the most pronounced peak is now at about 275 eV, while the  $\pi$  maximum has shifted down in energy to 281 eV. There are less dramat-

ic changes when the excitation energy is increased further, but one can see changes both in the  $\sigma$  and the  $\pi$  components of the emission. In selectively excited XES of amorphous carbon, on the other hand, there are only minor variations.<sup>24</sup> The difference in behavior between HOPG and amorphous carbon and the observation of similar differences between crystalline and amorphous silicon<sup>25,26</sup> suggest that the dependence on excitation energy is related to the presence of crystallographic order in the system.

The dependence on excitation energy observed here for HOPG is similar to what has been observed for diamond.<sup>3</sup> For diamond, the variations in the spectra could be successfully explained using a scattering approach, where the emission is considered not as a two-step process (absorption followed by emission), but as a one-step RIXS process.<sup>3,4</sup> This approach has also been used to describe the variations of the x-ray emission of solid C<sub>60</sub> in a molecular picture.<sup>27</sup> Here we shall interpret the fluorescence spectra within a RIXS formalism for the band structure of graphite.

Momentum must be conserved in resonant inelastic scattering, as described by

$$(\mathbf{k}_v - \mathbf{k}_e + \mathbf{q}_a - \mathbf{q}_b + \mathbf{G}) = 0. \quad (1)$$

The momenta of the photons,  $\mathbf{q}_a$  and  $\mathbf{q}_b$ , for soft x rays are quite small and normally much less than those of the electrons. They can therefore be neglected. Thus the difference between the momentum of the valence hole state,  $\mathbf{k}_v$ , and the momentum of the photoelectron,  $\mathbf{k}_e$ , equals a reciprocal lattice vector  $\mathbf{G}$ . The incident photons promote the core electron to an unoccupied state with the momentum  $\mathbf{k}_e$ . The emission in the scattering approach takes place, due to the momentum conservation, from occupied states that have momentum  $\mathbf{k}_e + \mathbf{G}$ . The scattering process can thus be viewed as a vertical electronic transition between the valence and the conduction band. Hence the emission will occur from those critical points that have a high DOS in the energy region selected by the exciting photon beam.

To obtain the RIXS intensity from the emission data, we assume in accordance with the previous work on diamond<sup>3</sup> that the fluorescence spectrum consists of a coherent part, for which the momentum is conserved, and an incoherent part, with a shape that is independent of the excitation energy. We assume that the high-energy-excited fluorescence spectrum (we used an excitation by 400 eV photons) can be used as the incoherent part of the spectrum. To determine the coherent part, first we subtract a linear background from each spectrum and then subtract a certain amount of the high-energy-excited spectrum that has been recorded at the same angle of incidence. The amount subtracted depends upon the excitation energy, and is chosen so that no negative features appear in the difference spectrum. Using this method, the fraction of the coherent part in our spectra decreased from about 0.5 for those recorded with excitation close to the C K edge to about 0.2 for excitation approximately 20 eV above the C K edge.

To obtain the  $\sigma$  and  $\pi$  contributions of the coherent part of the emission, spectra recorded at two extreme angles were used. We first extracted the coherent part of the spectra as described in the previous section. The  $\pi$  contribution was then obtained by normalizing the spectra recorded at the two extreme angles (12° and 72°) so that they have the same intensity in the low-energy part and then taking the difference between these two spectra. The  $\pi$  contribution obtained in this way was in turn normalized to the high-energy side of one of the spectra used, assuming only  $\pi$  states in the high-energy region, in agreement with Ref. 17. To check the validity of this procedure, a spectrum derived for 32° was calculated using the dipole approximation.<sup>9</sup> For those energies at which fluorescence spectra were recorded at an angle of 32°, the coherent part compares reasonably well to the simulated spectra. In Figs. 3(a) and 3(b) we show the result for the extracted  $\sigma$  and  $\pi$  contributions for three excitation energies. The labeling in Fig. 3 refers to the different excitation energies used and is the same as in Fig. 2.

The dependence on excitation energy can be explained qualitatively by first identifying, for each excitation energy, which critical points of the band structure can be reached. A band-structure calculation by Willis, Fitton,

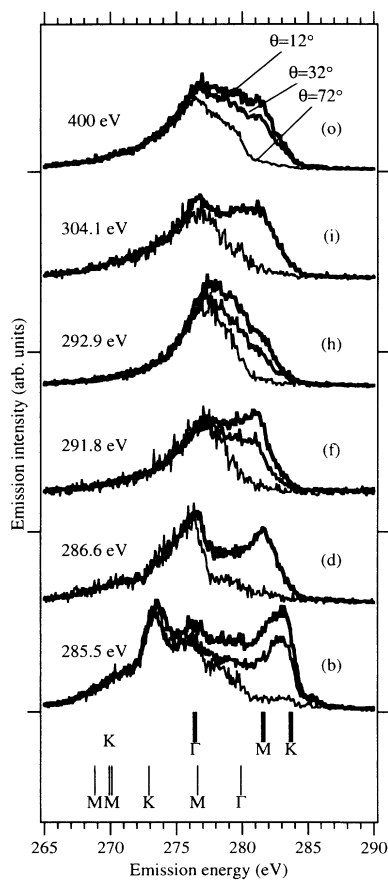


FIG. 2. Emission spectra recorded with different incidence angles and excitation energies as indicated in the figure. Indicated with bars are the energy positions of a number of critical points in the valence band taken from angle-resolved photoemission (Ref. 16). The thicker bars indicate critical points with  $\pi$  symmetry and the thinner  $\sigma$  symmetry.

and Painter<sup>22</sup> and the assignment of features in absorption spectra made by Rosenberg Love, and Rehn<sup>13</sup> have been used for the identification of the features in our absorption spectra. Critical points for the unoccupied states are labeled in the absorption spectra in Fig. 1. The energy positions of a set of critical points in the valence band using the Bouckaert-Smoluchowski-Wigner notation<sup>28</sup> are indicated in Figs. 2 and 3. The energy positions of the valence-band points are calculated using the experimental binding energies at the critical points taken from ARPES data<sup>16</sup> by subtracting them from the binding energy of the core hole, 284.4 eV.<sup>6</sup>

The  $\sigma$  and  $\pi$  contributions to the coherent part of the spectra recorded at 285.5 eV excitation energy are displayed in Figs. 3(a) and 3(b), respectively. At this energy, the photoelectron can only be promoted to the lower part of the conduction band. This region corresponds to  $\pi$  states with the  $k$  vector at the  $K$ - $H$  symmetry line in the band diagram.<sup>13</sup> Following the RIXS approach, enhanced scattering from states with the same momentum should be detected, i.e., from states at the  $K$ -

$H$  line in the occupied region of the valence band. For the  $\sigma$  valence band, there are states at the  $K$  point with binding energies 14.5 and  $\sim 11$  eV.<sup>16</sup> As seen in Fig. 3(a), there is a large increase in the  $\sigma$  component of the scattering at the corresponding emission energies. For the  $\pi$  states the states at the  $K$  point are close to the Fermi level. Here too, one observes enhanced scattering intensity [Fig. 3(b)]. For an excitation energy of 286.6 eV, the photoelectrons are restricted to states closer to the  $M$  point. The scattering intensity would then be high from points with  $M$  symmetry, as can be seen clearly in the spectra labeled  $d$  in Fig. 3. The spectra labeled  $h$  are the coherent part for an excitation energy of 292.9 eV. At this energy, the core electron is promoted to the  $\sigma$  states at both the  $\Gamma$  and the  $M$  points. For both the  $\sigma$  and  $\pi$  contributions, we would expect broader features because of the DOS distribution at the two critical points that can be reached in the excitation (the states with  $\Gamma$  and  $M$  symmetry further down in the band are not expected to contribute very much due to their low  $p$  character). This indicates the problem that occurs when sampling a large area of the Brillouin zone with the exciting beam. An excitation source with even narrower bandwidth may reveal more details for bands that are this close in energy. Following the changes of the spectral profiles of the other spectra one can see a clear correlation between the absorption and emission as described above.

To better compare experiment and theory, calculations must take into account the DOS for both valence and conduction bands. Such a calculation has been carried out for diamond,<sup>4</sup> where the shape of the RIXS component of the fluorescence spectra is well reproduced by the calculation. To be able to properly study a material like graphite with a large number of bands with small dispersion there is a need for higher resolution in both the excitation and the emission.

Finally, some comment on the implications of our results should be made. If one can use RIXS to obtain band-structure information, it would be especially valuable because it would be possible to make use of the advantages of XES compared to other spectroscopies. This would allow the investigation of insulating samples where the use of standard ARPES methods is not practical. RIXS would also have the advantage that true bulk properties and buried interfacial layers can be probed due to the large penetration and escape depth of the photons.

#### IV. CONCLUSIONS

We have measured angle-resolved x-ray absorption and x-ray fluorescence of HOPG. The variations of excitation energy in the fluorescence spectra can be interpreted in terms of resonant inelastic x-ray scattering and we show that, by applying this technique to a material with anisotropic crystal structure, symmetry-resolved band information can be obtained.

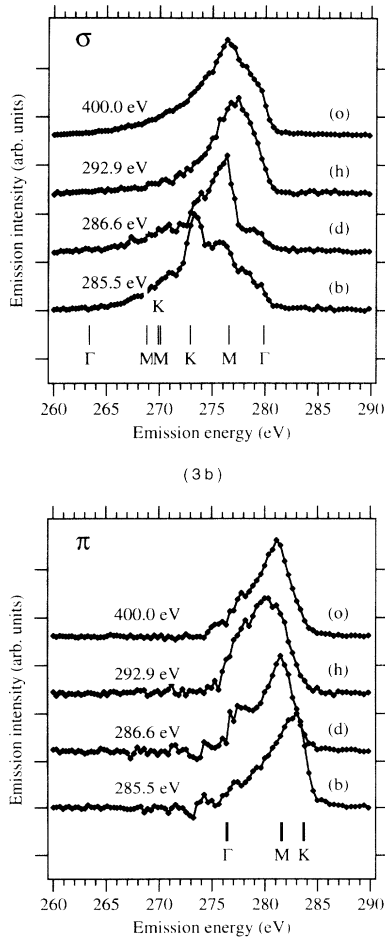


FIG. 3. The  $\pi$  and  $\sigma$  resolved coherent parts of the emission for different excitation energies representing the resonant-inelastic-scattering contribution of the emission. Indicated with bars are the energy positions of a number of critical points in the valence band taken from angle-resolved photoemission (Ref. 16).

## ACKNOWLEDGMENTS

We would like to thank E. Johansson and J.-O. Carlson for providing the samples. This work is supported in part by the Ångström Consortium for Thin Film Processes,

the Swedish Natural Science Research Council (NFR), and by the Göran Gustafssons Foundation for Research in Natural Sciences and Medicine. The National Synchrotron Light Source is operated under DOE Contract No. DE-AC02-76CH00016.

- 
- <sup>1</sup>*Angle Resolved Photoemission*, edited by S. D. Kevan (Elsevier, Amsterdam, 1992).
- <sup>2</sup>W. Schülke, U. Bonse, H. Nagasawa, A. Kaproiat, and A. Berthold, *Phys. Rev. B* **38**, 2112 (1988).
- <sup>3</sup>Y. Ma, N. Wassdahl, P. Skytt, J. Guo, J. Nordgren, P. D. Johnson, J.-E. Rubensson, T. Böske, W. Eberhardt, and S. D. Kevan, *Phys. Rev. Lett.* **69**, 2598 (1992).
- <sup>4</sup>P. D. Johnson and Y. Ma, *Phys. Rev. B* **49**, 5024 (1994); Y. Ma, *ibid.* **49**, 5799 (1994).
- <sup>5</sup>T. Åberg and B. Crasemann, in *X-ray Resonant (Anomalous) Scattering*, edited by K. Fischer, G. Materlik, and C. Sparks (Elsevier, Amsterdam, 1994), and references therein.
- <sup>6</sup>F. R. McFeely, S. P. Kowalczyk, L. Ley, R. G. Cavell, R. A. Pollak, and D. A. Shirley, *Phys. Rev. B* **9**, 5268 (1974).
- <sup>7</sup>A. Bianconi, S. B. M. Hagström, and R. Z. Bachrach, *Phys. Rev. B* **16**, 5543 (1977).
- <sup>8</sup>J. E. Fabian, in *Soft X-Ray Band Spectroscopy and Electronic Structure of Metals and Materials*, edited by D. J. Fabian (Academic, New York, 1968), p. 118.
- <sup>9</sup>G. Wiech, in *Emission and Scattering Techniques*, edited by Peter Day (Reidel, Dordrecht, 1981), p. 103.
- <sup>10</sup>F. Maeda, T. Takahashi, H. Ohsawa, S. Suzuki, and H. Suemitsu, *Phys. Rev. B* **37**, 4482 (1988).
- <sup>11</sup>I. R. Collins, P. T. Andrews, and R. A. Law, *Phys. Rev. B* **38**, 13 348 (1988).
- <sup>12</sup>D. A. Fisher, R. M. Wentzcovitch, R. G. Carr, A. Continenza, and A. J. Freeman, *Phys. Rev. B* **44**, 1427 (1991).
- <sup>13</sup>R. A. Rosenberg, P. J. Love, and Victor Rehn, *Phys. Rev. B* **33**, 4034 (1986).
- <sup>14</sup>L. J. Terminello, D. K. Shuh, F. J. Himpsel, D. A. Lapiano-Smith, J. Stöhr, D. S. Bethune, and G. Meijer, *Chem. Phys. Lett.* **182**, 491 (1993).
- <sup>15</sup>P. E. Batson, *Phys. Rev. B* **48**, 2608 (1993).
- <sup>16</sup>A. R. Law, M. T. Johnson, and H. P. Hughes, *Phys. Rev. B* **34**, 4289 (1986).
- <sup>17</sup>X. Weng, P. Rez, and H. Ma, *Phys. Rev. B* **40**, 4175 (1989).
- <sup>18</sup>R. C. Tatar and S. Rabii, *Phys. Rev. B* **25**, 4126 (1982).
- <sup>19</sup>J.-C. Charlier, J.-P. Michenaud, and X. Gonze, *Phys. Rev. B* **46**, 4531 (1992).
- <sup>20</sup>K. J. Randall, J. Feldhaus, W. Ehlebach, A. M. Bradshaw, W. Eberhardt, Z. Xu, Y. Ma, and P. D. Johnson, *Rev. Sci. Instrum.* **63**, 1367 (1992).
- <sup>21</sup>J. Nordgren and R. Nyholm, *Nucl. Instrum. Methods Phys. Res. Sect. A* **246**, 242 (1986); J. Nordgren, G. Bray, S. Cramm, R. Nyholm, J.-E. Rubensson, and N. Wassdahl, *Rev. Sci. Instrum.* **60**, 1690 (1989).
- <sup>22</sup>R. T. Willis, B. Fitton, and G. S. Painter, *Phys. Rev. B* **9**, 1926 (1974).
- <sup>23</sup>Y. Ma, P. Skytt, N. Wassdahl, P. Glans, J. Guo, D. C. Mancini, and J. Nordgren, *Phys. Rev. Lett.* **71**, 3725 (1993).
- <sup>24</sup>P. Skytt, P. Glans, D. C. Mancini, J.-H. Guo, N. Wassdahl, and J. Nordgren (unpublished).
- <sup>25</sup>J.-E. Rubensson, D. Mueller, R. Shuker, D. L. Ederer, C. H. Zhang, J. Jia, and T. A. Calcott, *Phys. Rev. Lett.* **64**, 1047 (1990).
- <sup>26</sup>K. E. Miyano, D. L. Ederer, T. A. Calcott, Y. Ma, J. C. Woicik, D. R. Mueller, W. L. O'Brian, J. J. Jia, L. Zhou, and Q.-Y. Dong, *Phys. Rev. B* **48**, 1918 (1993).
- <sup>27</sup>J.-H. Guo, P. Glans, P. Skytt, N. Wassdahl, J. Nordgren, Y. Ma, Y. Luo, and H. Ågren (unpublished).
- <sup>28</sup>L. P. Bouckaert, R. Smoluchowski, and E. Wigner, *Phys. Rev.* **50**, 56 (1936).